

PAPER • OPEN ACCESS

On the dynamics of five- and six-dimensional Lorenz models

To cite this article: Carolini C Felicio and Paulo C Rech 2018 *J. Phys. Commun.* **2** 025028

View the [article online](#) for updates and enhancements.

You may also like

- [Analytic proof of the existence of the Lorenz attractor in the extended Lorenz model](#)
I I Ovsyannikov and D V Turaev
- [Systematics of the Periodic Windows in the Lorenz Model and its Relation with the Antisymmetric Cubic Map](#)
Ding Ming-zhou and Hao Bai-lin
- [Wild pseudohyperbolic attractor in a four-dimensional Lorenz system](#)
Sergey Gonchenko, Alexey Kazakov and Dmitry Turaev

Journal of Physics Communications



OPEN ACCESS

PAPER

On the dynamics of five- and six-dimensional Lorenz models

Carolini C Felicio and Paulo C Rech

Departamento de Física, Universidade do Estado de Santa Catarina, 89219-710 Joinville, Brazil

E-mail: paulo.rech@udesc.br

Keywords: Lorenz model, 5D Lorenz model, 6D Lorenz model, Lyapunov exponents spectra, parameter planesRECEIVED
16 November 2017REVISED
2 January 2018ACCEPTED FOR PUBLICATION
19 January 2018PUBLISHED
21 February 2018

Original content from this work may be used under the terms of the Creative Commons Attribution 3.0 licence.

Any further distribution of this work must maintain attribution to the author(s) and the title of the work, journal citation and DOI.

**Abstract**

In this paper we report on generalized Lorenz models. Five- and six-dimensional Lorenz models are investigated, which are obtained by considering respectively two and three additional Fourier modes in addition to the modes included in the derivation of the classical three-dimensional Lorenz model. Parameter planes, bifurcation diagrams, and attractors in the phase-space are used, in order to investigate the influence of the additional Fourier modes on solutions, when compared with the solutions for the classical Lorenz model. It is shown that for parameters σ and b kept fixed, a larger parameter r results for the onset of chaos in five- and six-dimensional Lorenz models. Also it is shown that the shape of bifurcation diagrams, periodic, and chaotic attractors is preserved in both generalized Lorenz models. Additionally, it is shown that hyperchaos is observed only in the six-dimensional Lorenz model, at least in the parameter ranges here investigated.

1. Introduction

The classical Lorenz system [1, 2] given by

$$\begin{aligned}\dot{x} &= \sigma y - \sigma x, \\ \dot{y} &= rx - y - xz, \\ \dot{z} &= xy - bz,\end{aligned}\tag{1}$$

is a mathematical model for a two-dimensional Rayleigh-Bénard thermal convection of a fluid, which is contained between two plates placed in a direction perpendicular to the Earth's gravitational force, heated from below and cooled from above. A very didactical discussion concerning the physical meaning of the dynamical variables x , y , z , and parameters b , r , σ , can be seen in Dullin and co-workers [3]. Our aim in this section is to report a very brief review of the three-dimensional Lorenz model (3LM), from the viewpoint of three different parameter planes, namely (r, σ) , (r, b) , and (σ, b) .

Parameter plane diagrams are important because they may be interpreted as cross sections of a n -dimensional parameter-space of a system with more than two control parameters. Such diagrams allow us to observe regular (periodic or quasiperiodic) and chaotic orbits on continuous sets of parameters. This knowledge of the organization of chaos and regularity in parameter planes may be useful to choose suitable paths in the parameter-space. For instance, by making appropriate modifications in parameters, we can travel over domains where the system is always chaotic, which is interesting for practical applications involving for example chaos control, chaotic secure communication and chaotic synchronization. Parameter planes of different continuous-time nonlinear mathematical models has been the subject of several recent publications. Some few examples consider the Rössler oscillator [4], a chemical oscillator [5], electronic circuits [5–8], semiconductor lasers [9–11], a Hopfield neural network [12], an ecological model [13], a tumor growth model [14], a damped-forced oscillator [15], a driven Josephson junction [16], the time evolution of finite-amplitude gravity waves in a rotating atmosphere [17], a non-ideal Duffing oscillator [18], a controlled Lorenz system [19], a radio-physical oscillator [20], and a Van der Pol-Duffing oscillator [21].

Therefore, a parameter plane of the 3LM, a cross section of their three-dimensional (b, r, σ) parameter-space, is a diagram that shows regions of different dynamical behaviors, namely equilibrium point, chaos, and regularity, depending on parameters. There is more than one way to characterize the dynamical behavior of each point in a parameter plane. Here we use numerical estimates of the Lyapunov exponents spectrum obtained by

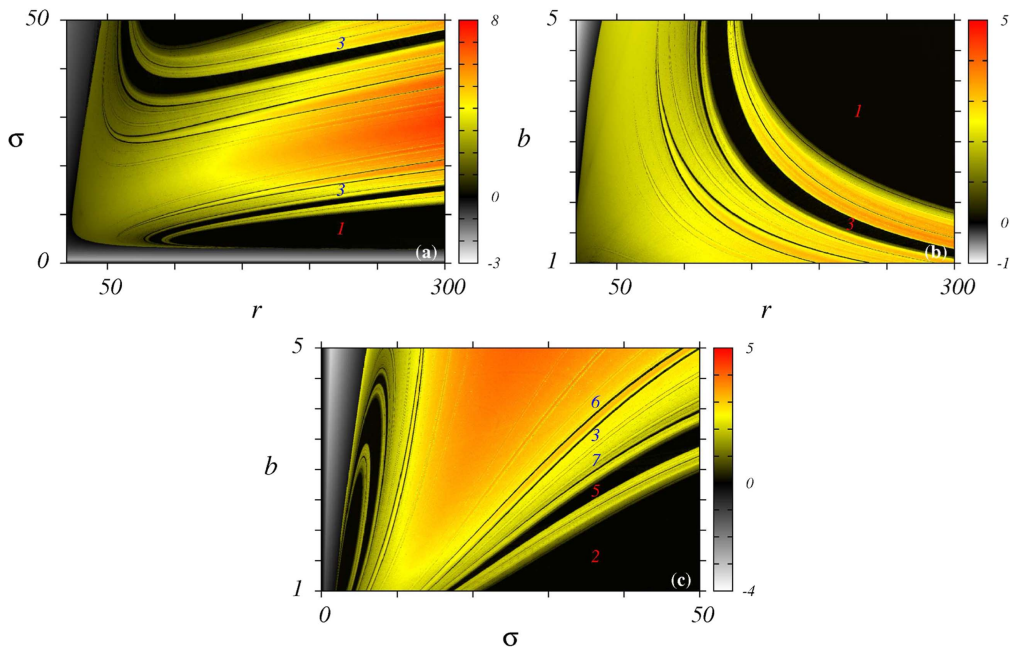


Figure 1. Stability domains in parameter planes of system (1). Color is related to the magnitude of the largest Lyapunov exponent. (a) The (r, σ) parameter plane, for $b = 8/3$. (b) The (r, b) parameter plane, for $\sigma = 10$. (c) The (σ, b) parameter plane, for $r = 100$.

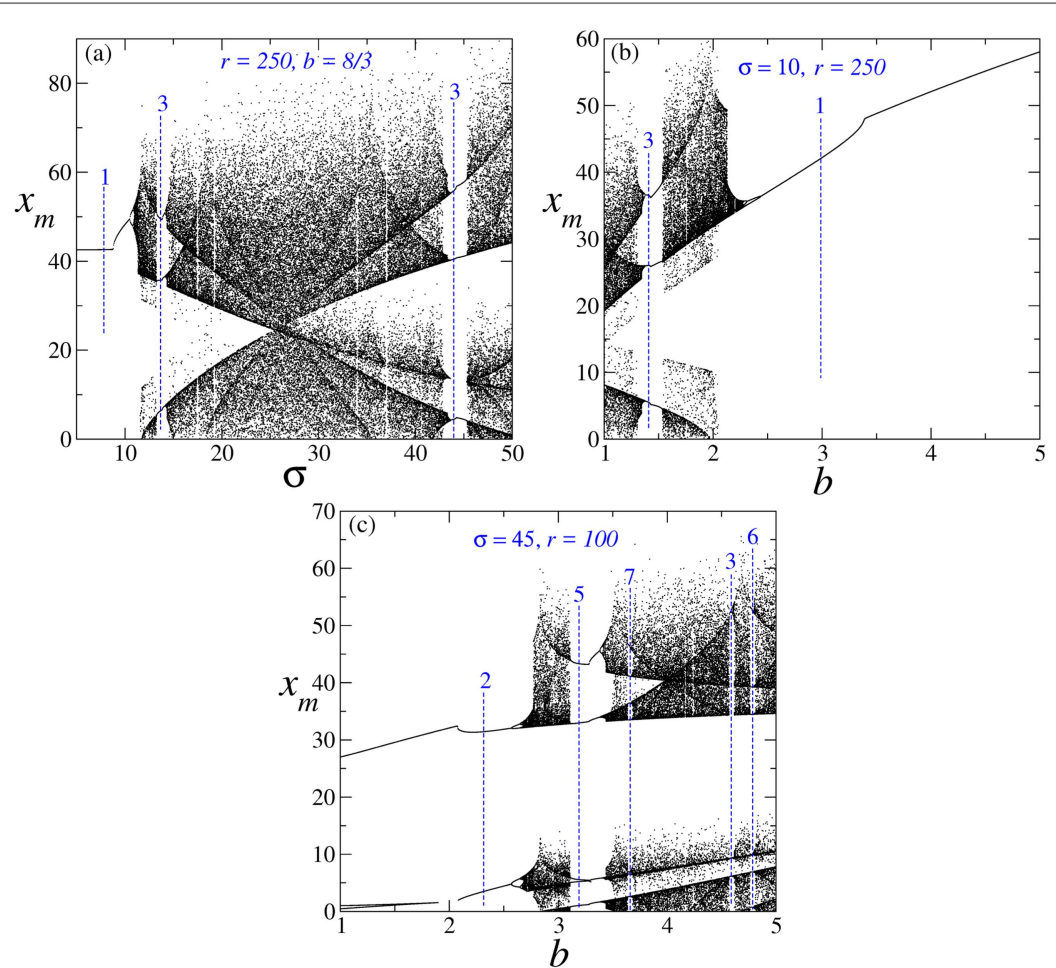


Figure 2. (a) Bifurcation diagrams for system (1). Plotted are the local maxima of the variable x , represented by x_m . (a) Are considered points along the line $r = 250$ in figure 1(a), with $b = 8/3$. (b) Are considered points along the line $r = 250$ in figure 1(b), with $\sigma = 10$. (c) Are considered points along the line $\sigma = 45$ in figure 1(c), with $r = 100$.

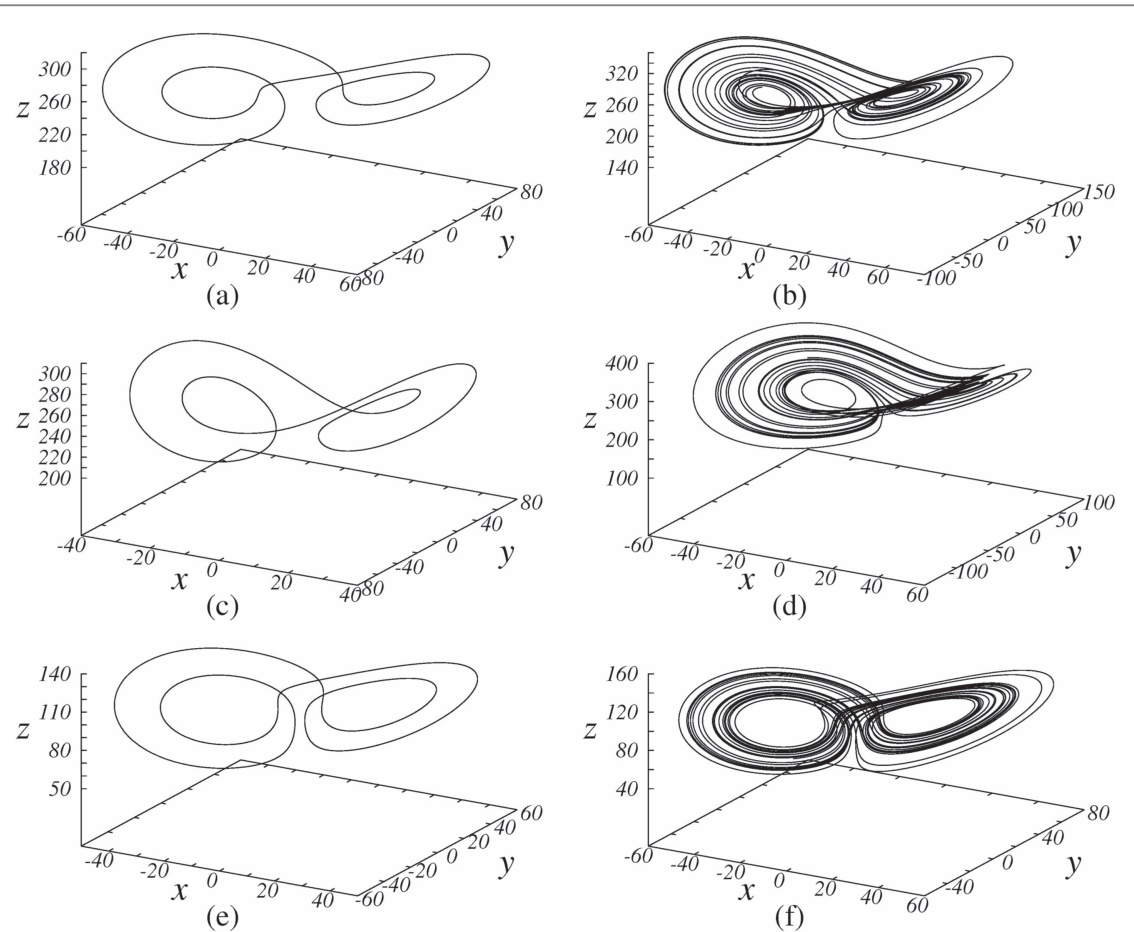


Figure 3. Six attractors related to the Lorenz system (1). (a), (c), and (e) Periodic trajectories, corresponding respectively to a point in the more prominent stripe in figures 1(a), (b), and (c) (see text). (b), (d), and (f) Chaotic trajectories, corresponding respectively to a point in the yellow to red region in figures 1(a), (b), and (c) (see text).

using the algorithm presented in Wolf and co-workers [22], and in the specific case of the 3LM only the largest Lyapunov exponent (LLE) is considered. Our understanding regarding the interpretation of the value of the LLE (positive, negative, or zero) is based on the work by Wolf and co-workers [22], although we know that a negative LLE does not indicate, in general, stability, as well as a positive LLE does not indicate, in general, instability [23]. Hence, a negative LLE is related with an equilibrium point, a positive LLE corresponds to a chaotic behavior, and a zero LLE means periodicity (or quasiperiodicity, when the second LLE also is null).

Before we present the three parameter planes for the 3LM, we explain in the following how these diagrams are obtained. Regardless of which are the two considered parameters in the diagram, is considered the LLE value in each point of a $10^3 \times 10^3$ grid of equally spaced points. Prior to the calculation of each LLE, the Lorenz system (1) is numerically integrated by using a fourth order Runge-Kutta algorithm [24], with a fixed time step size equal to 10^{-4} , being dropped the first 1×10^6 integration steps, regarded as a transient. For the computation of the average involved in the calculation of each one of the 1×10^6 LLE, were considered the subsequent 1×10^6 integration steps.

Integration of equations (1) was performed always from the initial condition $(x_0, y_0, z_0) = (0.1, 0.2, 0.3)$.

Figure 1 shows in (a) the (r, σ) parameter plane for $b = 8/3$, in (b) the (r, b) parameter plane for $\sigma = 10$, and in (c) the (σ, b) parameter plane for $r = 100$. Similar diagrams have been reported before [3, 25, 26], even considering other parameters ranges, and even other tools to characterize the dynamical behavior of each point in the respective parameter plane. Color in diagrams of figure 1 is related to the magnitude of the respective LLE. A positive LLE is indicated by a continuously changing yellow to red color, a negative LLE is indicated by a continuously changing white to black color, and the black color itself indicates a zero LLE, according to the scale shown in the column at right side in each diagram. Therefore, regardless of the considered diagram in figure 1, we can see a large chaotic region, as well as equilibrium point and periodic regions. Embedded in the yellow to red chaotic region we observe periodic stripes in black, the most visible identified with a number that means the period of the respective stripe.

Numbers signifying periods of some stripes in diagrams of figure 1 were obtained from the bifurcation diagrams in figure 2, which consider 10^3 values of the respective parameter in the horizontal axis. Diagram in figure 2(a) was constructed by varying σ along the line $r = 250$ in figure 1(a), that in figure 2(b) considers the

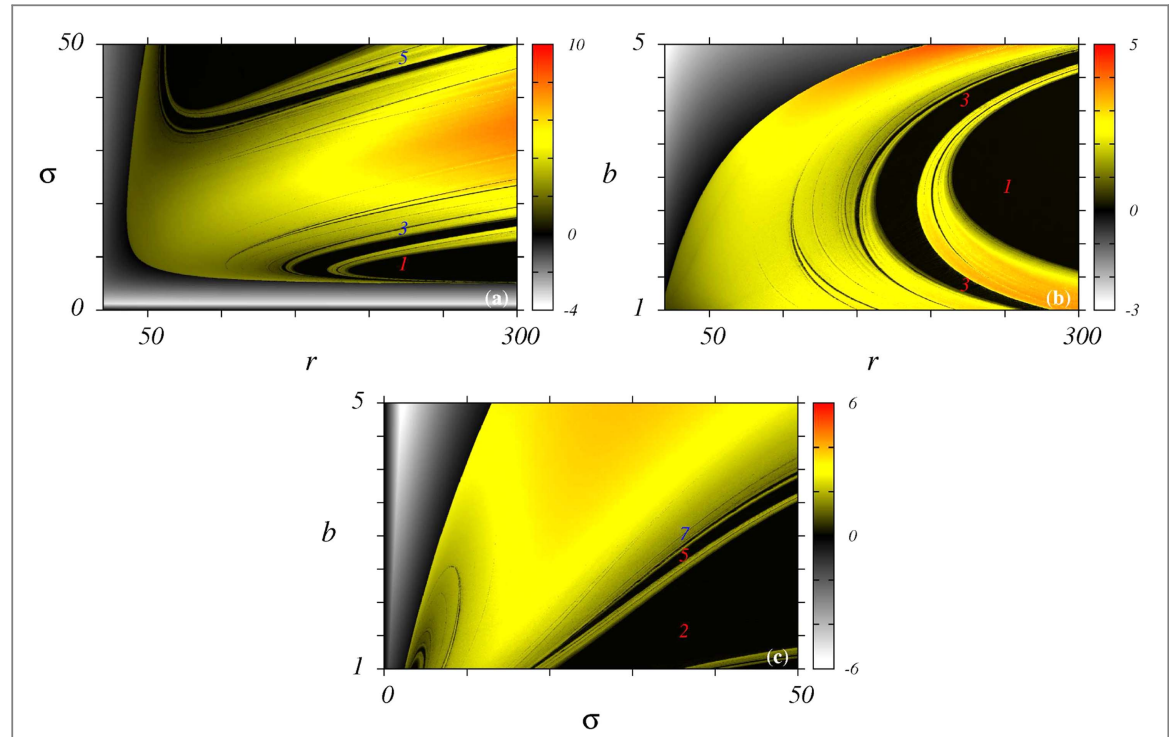


Figure 4. Stability domains in parameter planes of system (2). Color is related to the magnitude of the largest Lyapunov exponent. (a) The (r, σ) parameter plane, for $b = 8/3$. (b) The (r, b) parameter plane, for $\sigma = 10$. (c) The (σ, b) parameter plane, for $r = 100$.

variation of b along the line $r = 250$ in figure 1(b), while that in figure 2(c) refer to the variation of b along the line $\sigma = 45$ in figure 1(c). Numerical integrations involved in the solution of the set of ordinary differential equations were performed by using the fourth-order Runge-Kutta method, with a time step size 10^{-4} . In each diagram of figure 2 is represented the number of local maxima of the variable x , denoted by x_m , in one complete trajectory on the phase-space attractor, as a function of the respective parameter. Notice that for each numbered window of periodicity in diagrams of figure 2, there is an associated periodic structure (a stripe) in the related diagram of figure 1.

Figure 3 shows typical periodic and two-wing chaotic attractors in the phase-space of the Lorenz system (1). Periodic attractors are shown in figures 3(a), (c), and (e) for which $(b, r, \sigma) = (8/3, 250, 44)$, $(b, r, \sigma) = (1.4, 250, 10)$, and $(b, r, \sigma) = (3.3, 100, 45)$, respectively. Each of these sets of parameters locate a point in the more prominent black stripe of each of the diagrams in figure 1. Two-wing chaotic attractors are shown in figures 3(b), (d), and (f). Such chaotic attractors are corresponding to the points $(b, r, \sigma) = (8/3, 250, 20)$, $(b, r, \sigma) = (1.9, 250, 10)$, and $(b, r, \sigma) = (4.4, 100, 45)$, located respectively in the yellow to red region of the same diagrams in figure 1. For the construction of each periodic trajectory in figure 3 were considered 20×10^3 integration steps, after an adequate transient, while each chaotic trajectory consider 10×10^4 integration steps.

We would like to point out that the 3LM is one of the most well-studied systems [27] in the nonlinear dynamics field. Therefore, none of the above results is new. As mentioned before, the principal objective in this work is to compare parameter planes of five- and six-dimensional Lorenz models, with the ones of the original Lorenz model (1). This is the motivation for the presence of figures 1, 2, and 3 in this paper, which is organized as follows. Section 2.1 is dedicated to the five-dimensional Lorenz model (5LM), while the six-dimensional Lorenz model (6LM) is considered in section 2.2. Additionally, the possibility of hyperchaos in the two generalized Lorenz systems is investigated in section 2.3. Finally, the paper is summarized in section 3.

2. Results discussion

2.1. The five-dimensional Lorenz model

The 3LM, modeled by equations (1), was obtained by considering three Fourier modes to represent the streamfunction and temperature perturbations in the thermal convection process. The five-dimensional Lorenz model [28] given by

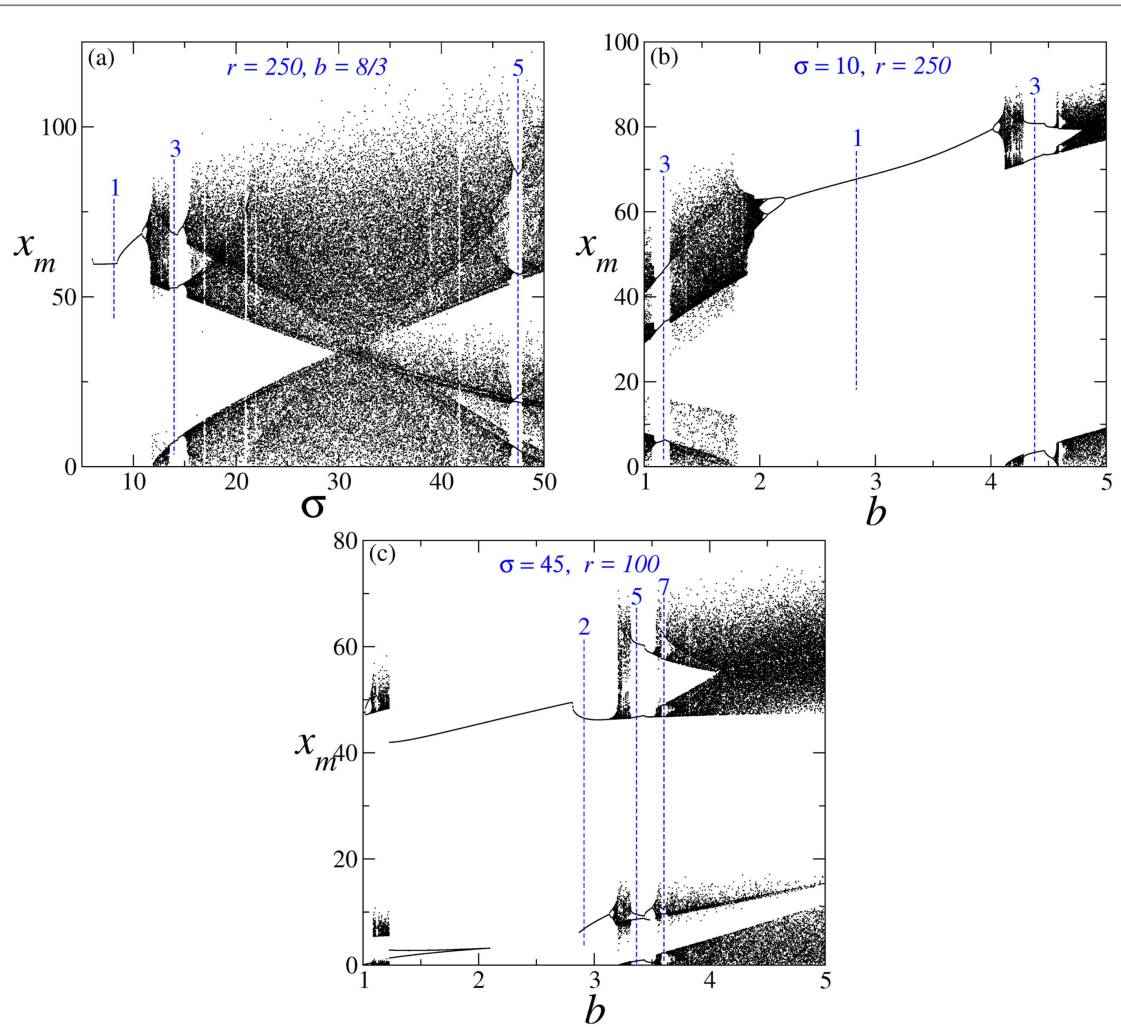


Figure 5. (a) Bifurcation diagrams for system (2). Plotted are the local maxima of the variable x , represented by x_m . (a) Are considered points along the line $r = 250$ in figure 4(a), with $b = 8/3$. (b) Are considered points along the line $r = 250$ in figure 4(b), with $\sigma = 10$. (c) Are considered points along the line $\sigma = 45$ in figure 4(c), with $r = 100$.

$$\begin{aligned} \dot{x} &= \sigma(y - x), \\ \dot{y} &= rx - y - xz, \\ \dot{z} &= xy - bz - xv, \\ \dot{v} &= xz - 2xu - (1 + 2b)v, \\ \dot{u} &= 2xv - 4bu, \end{aligned} \quad (2)$$

considers two additional Fourier modes. We can see that two new dynamical variables, v and u , and two new first-order ordinary differential equations are added, when the comparison is made with equations (1). Also added are two new nonlinearities, namely xv in \dot{z} and \dot{u} equations and xu in the \dot{v} equation. Based on the understanding that the origin of chaos is in the nonlinearities, is expected that solutions for system (2) become more chaotic than those solutions for system (1). We will check this in the continuation. Before that, notice that model (1) can be obtained from model (2), if we neglect the variables v and u .

Figure 4 shows in (a) the (r, σ) parameter plane for $b = 8/3$, in (b) the (r, b) parameter plane for $\sigma = 10$, and in (c) the (σ, b) parameter plane for $r = 100$. All the diagrams in figure 4 are related with the 5LM, and were obtained in an analogous manner as the ones in figure 1, with an additional initial condition $(v_0, u_0) = (0.4, 0.5)$ for the new variables v and u . As before in figure 1, color in diagrams of figure 4 is related to the magnitude of the LLE. Roughly speaking, the pictures in figure 4 are similar to those in figure 1. However, a closer look allows us to see differences. For example, the area covered by chaos is larger in diagram of figure 4 than in the corresponding diagram of figure 1. Several periodic stripes present in the 3LM are not present in the 5LM. The range of the LLE is increased, as well as their upper limit, except for the case involving the parameters (r, b) .

Concerning diagrams (a) and (b) in both figures 1 and 4, it can be seen that a larger r is necessary for the onset of chaos in the 5LM, when a comparison is made with the 3LM. For example, for $\sigma = 50$ and $b = 8/3$, $r = 46.08$ in the 3LM case, while $r = 49.18$ in the 5LM case, numbers obtained from figures 1(a) and 4(a), respectively. The

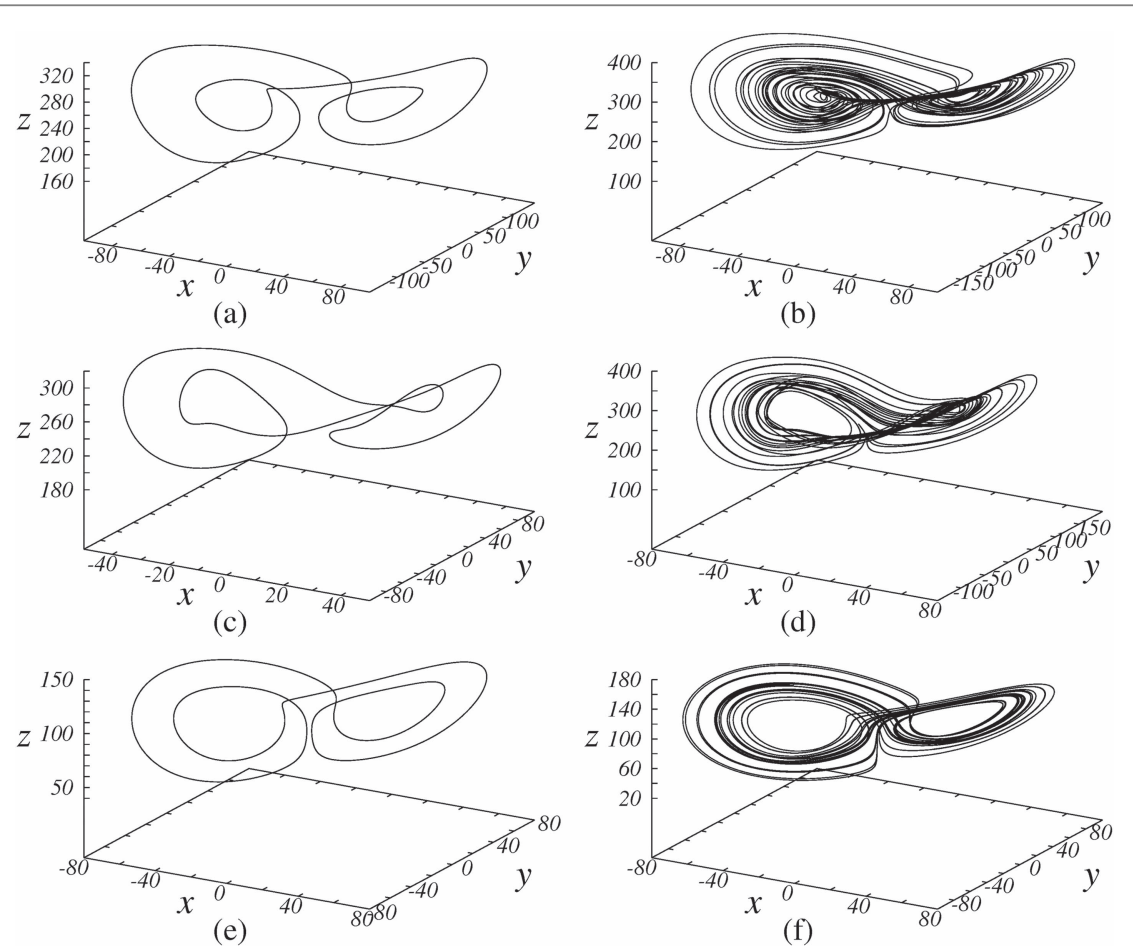


Figure 6. Six xyz projections of attractors related to the five-dimensional Lorenz system (2). (a), (c), and (e) Periodic trajectories, corresponding respectively to a point in the more prominent stripe in figures 4(a), (b), and (c) (see text). (b), (d), and (f) Chaotic trajectories, corresponding respectively to a point in the yellow to red region in figures 4(b), (d), and (f) (see text).

difference between the two values of r increases if one considers $\sigma = 10$ and $b = 5$. In this case, figures 1(b) and 4(b) give results $r = 39.29$ in the 3LM case, and $r = 197.52$ in the 5LM case. Considering σ as the bifurcation parameter, $b = 5$ and $r = 100$, figures 1(c) and 4(c) give as result $\sigma = 5.88$ and $\sigma = 12.96$ for the onset of chaos, respectively in the 3LM and in the 5LM.

All findings reported above are also supported when comparing the bifurcation diagrams in figure 2, related with the 3LM, with the ones in figure 5, related with the 5LM. As before in figure 2, diagram in figure 5(a) was constructed by varying σ along the line $r = 250$ in figure 4(a), diagram in figure 5(b) considers the variation of b along the line $r = 250$ in figure 4(b), and diagram in figure 5(c) refers to the variation of b along the line $\sigma = 45$ in figure 4(c). Again fourth-order Runge-Kutta method with a time step size 10^{-4} was used to perform the numerical integrations. By looking at the diagrams labeled with the same letter in figures 2 and 5 we can see that bifurcation diagrams related to the 5LM appear shifted to the right, although they are similar to the ones related to the 3LM. Therefore, regardless of which is the bifurcation parameter considered, the onset of chaos is delayed in the 5LM, when compared with the 3LM.

With respect to the shape of the attractors, figure 6 shows three-dimensional projections related to the 5LM. Projections of periodic attractors are shown in figures 6(a), (c), and (e) for which $(b, r, \sigma) = (8/3, 250, 47.5)$, $(b, r, \sigma) = (1.15, 250, 10)$, and $(b, r, \sigma) = (3.4, 100, 45)$, respectively. Each of these sets of parameters locate a point in the more prominent black stripe of each of the diagrams in figure 4. Projections of chaotic attractors are shown in figures 6(b), (d), and (f). They are corresponding to the points $(b, r, \sigma) = (8/3, 250, 30)$, $(b, r, \sigma) = (1.6, 250, 10)$, and $(b, r, \sigma) = (4.4, 100, 45)$, located respectively in the yellow to red region of the same diagrams in figure 4. As before in the case of the 3LM, for the construction of each periodic trajectory in figure 6 were considered 20×10^3 integration steps after an adequate transient, while each chaotic trajectory consider 10×10^4 integration steps. By comparing figures 3 and 6, a possible conclusion is that the shape of attractors is preserved, when we pass from the 3LM to the 5LM.

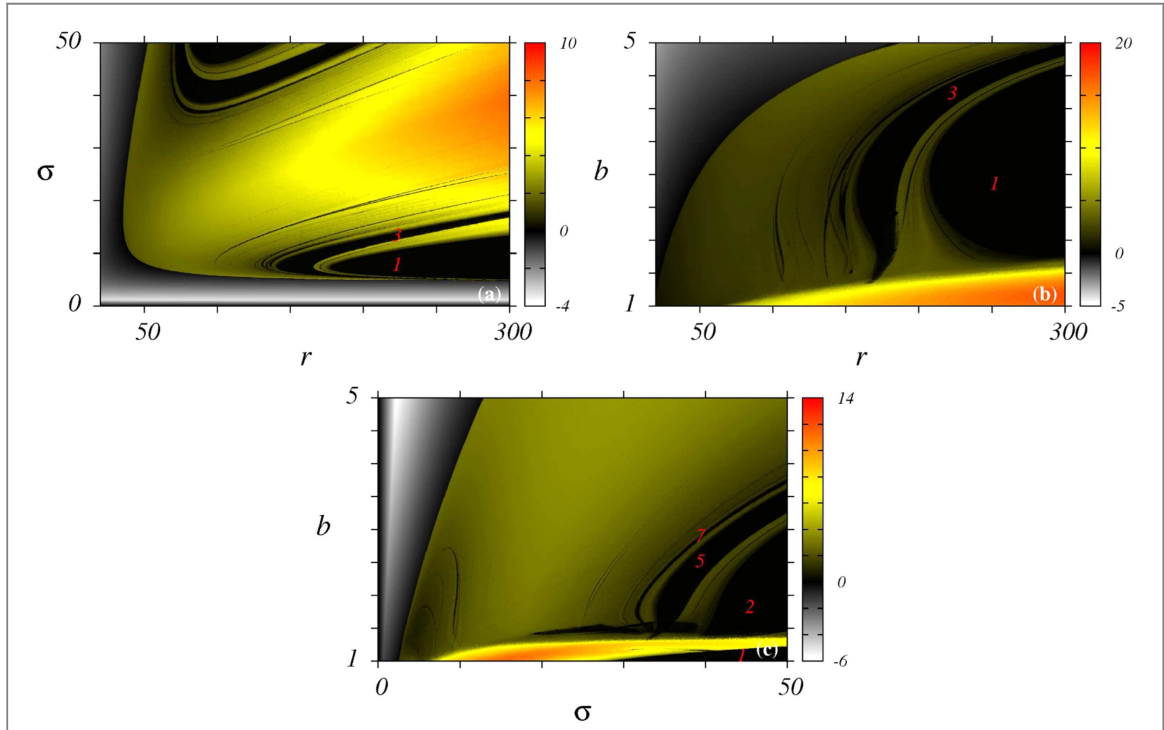


Figure 7. Stability domains in parameter planes of system (3). Color is related to the magnitude of the largest Lyapunov exponent. (a) The \$(r, \sigma)\$ parameter plane, for \$b = 8/3\$. (b) The \$(r, b)\$ parameter plane, for \$\sigma = 10\$. (c) The \$(\sigma, b)\$ parameter plane, for \$r = 100\$.

2.2. The six-dimensional Lorenz model

The six-dimensional Lorenz model [29] given by

$$\begin{aligned} \dot{x} &= \sigma(y - x), \\ \dot{y} &= rx - y - xz + zv - 2\nu\omega, \\ \dot{z} &= xy - bz - xu - yv, \\ \dot{v} &= -(1 + 2b)\sigma v + \frac{\sigma}{(1 + 2b)}u, \\ \dot{u} &= xz - 2x\omega + rv - (1 + 2b)u, \\ \dot{\omega} &= 2xu + 2yv - 4b\omega, \end{aligned} \quad (3)$$

takes into account an additional Fourier mode, in relation to the 5LM. As a consequence, a new dynamical variable, \$\omega\$, and a new first-order ordinary differential equation are added, when the comparison is made with equations (2). Also added are two new nonlinearities, namely \$yv\$ in \$\dot{z}\$ and \$\dot{\omega}\$ equations and \$x\omega\$ in the \$\dot{u}\$ equation. As happened before with model (2), notice that model (1) can be obtained from model (3), if we neglect the variables \$v\$, \$u\$, and \$\omega\$.

Figure 7 shows in (a) the \$(r, \sigma)\$ parameter plane for \$b = 8/3\$, in (b) the \$(r, b)\$ parameter plane for \$\sigma = 10\$, and in (c) the \$(\sigma, b)\$ parameter plane for \$r = 100\$. Diagrams in figure 7 refer to the 6LM, and were obtained in a similar way as the ones in figure 4, with an additional initial condition \$\omega_0 = 0.6\$ for the new variable \$\omega\$. As before in figures 1 and 4, color in diagrams of figure 7 is related to the magnitude of the LLE. The area covered by chaos is larger in diagrams of figure 7 than in the corresponding diagrams of figures 4 and 1. Again the range of the LLE is increased, as well as their upper limit, except for the case involving the parameters \$(r, \sigma)\$. In fact, it is remarkable the wide variation in the magnitude of the LLE for both \$(r, b)\$ and \$(\sigma, b)\$ parameter planes of the 6LM case, as well as their upper limit. Comparing with the 5LM case, the upper limit changed from 5 to 20 and from 6 to 14, respectively. As can be checked in figures 7(b) and (c), higher values to the magnitude of the LLE occur for values of the parameter \$b\$ close to the unity, namely in the more intense red region.

Figure 8 shows bifurcation diagrams related with the 6LM. Diagram in figure 8(a) was constructed by varying \$\sigma\$ along the line \$r = 250\$ in figure 7(a), diagram in figure 8(b) considers the variation of \$b\$ along the line \$r = 250\$ in figure 7(b), and diagram in figure 8(c) refers to the variation of \$b\$ along the line \$\sigma = 45\$ in figure 7(c). Again fourth-order Runge-Kutta method with a time step size \$10^{-4}\$ was used to perform the numerical integrations. Each of the diagrams in figure 8 is similar to the respective in figure 5, whose diagrams, as we know, are related to

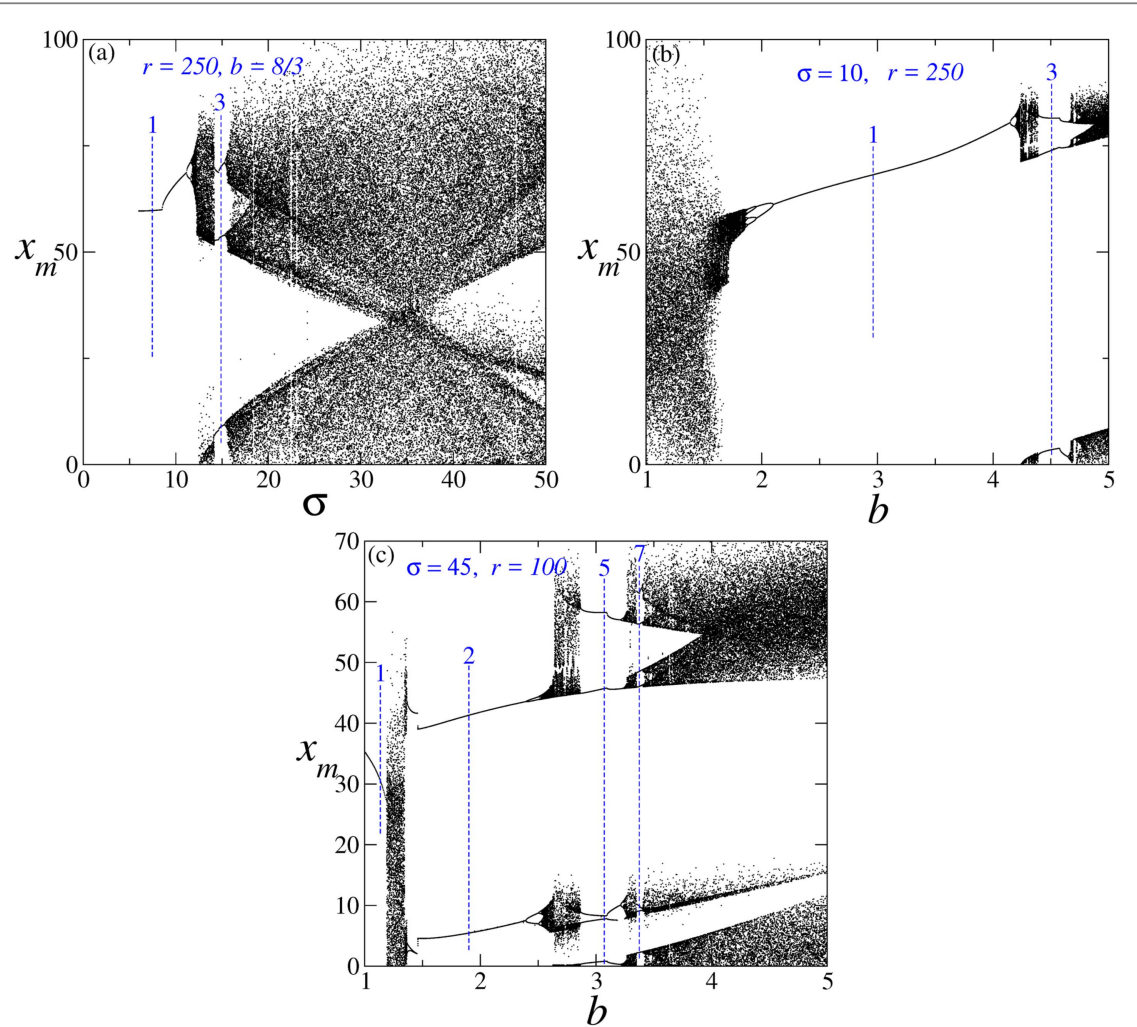


Figure 8. (a) Bifurcation diagrams for system (3). Plotted are the local maxima of the variable x , represented by x_m . (a) Are considered points along the line $r = 250$ in figure 7(a), with $b = 8/3$. (b) Are considered points along the line $r = 250$ in figure 7(b), with $\sigma = 10$. (c) Are considered points along the line $\sigma = 45$ in figure 7(c), with $r = 100$.

the 5LM case. There are, however, differences, that are due to the chaotic regions of higher values of the LLE in figures 8(b) and (c) we have mentioned above. The period-3 region in figure 5(b) and the period-1 region in figure 5(c) appear both as chaotic regions, respectively in figures 8(b) and (c).

The shape of the attractors does not change again, whether they are periodic or chaotic. Such fact can be checked in figure 9 that shows three-dimensional projections related to the 6LM. Projections of periodic attractors are shown in figures 9(a), (c), and (e) for which $(b, r, \sigma) = (8/3, 250, 8)$, $(b, r, \sigma) = (2.5, 250, 10)$, and $(b, r, \sigma) = (3.2, 100, 45)$, respectively. Each of these sets of parameters locate a point in some black region of each of the diagrams in figure 7. Projections of chaotic attractors are shown in figures 9(b), (d), and (f). They are corresponding to the points $(b, r, \sigma) = (8/3, 250, 30)$, $(b, r, \sigma) = (4.8, 250, 10)$, and $(b, r, \sigma) = (4.4, 100, 45)$, located in the yellow to red region of the same diagrams in figure 7. As before, for the construction of each periodic trajectory in figure 9 were considered 20×10^3 integration steps after an adequate transient, while each chaotic trajectory consider 10×10^4 integration steps.

2.3. Hyperchaos in five- and six-dimensional Lorenz models

In this section we use a method [30, 31] which considers alternative ways to numerically characterize regions with hyperchaotic behavior, in parameter planes of dynamical systems modeled by a set of at least four autonomous first-order nonlinear ordinary differential equations. The way used here takes into account the four (three) LLEs, to construct four (three) parameter plane plots for the 6LM (5LM), one for each of the four (three) Lyapunov exponents. With the understanding of a hyperchaotic system as being a chaotic system with at least two positive Lyapunov exponents, the possibility of hyperchaos with up to four (three) positive Lyapunov exponents can be investigated in system (3) (system (2)). Therefore, in order to investigate the possibility of

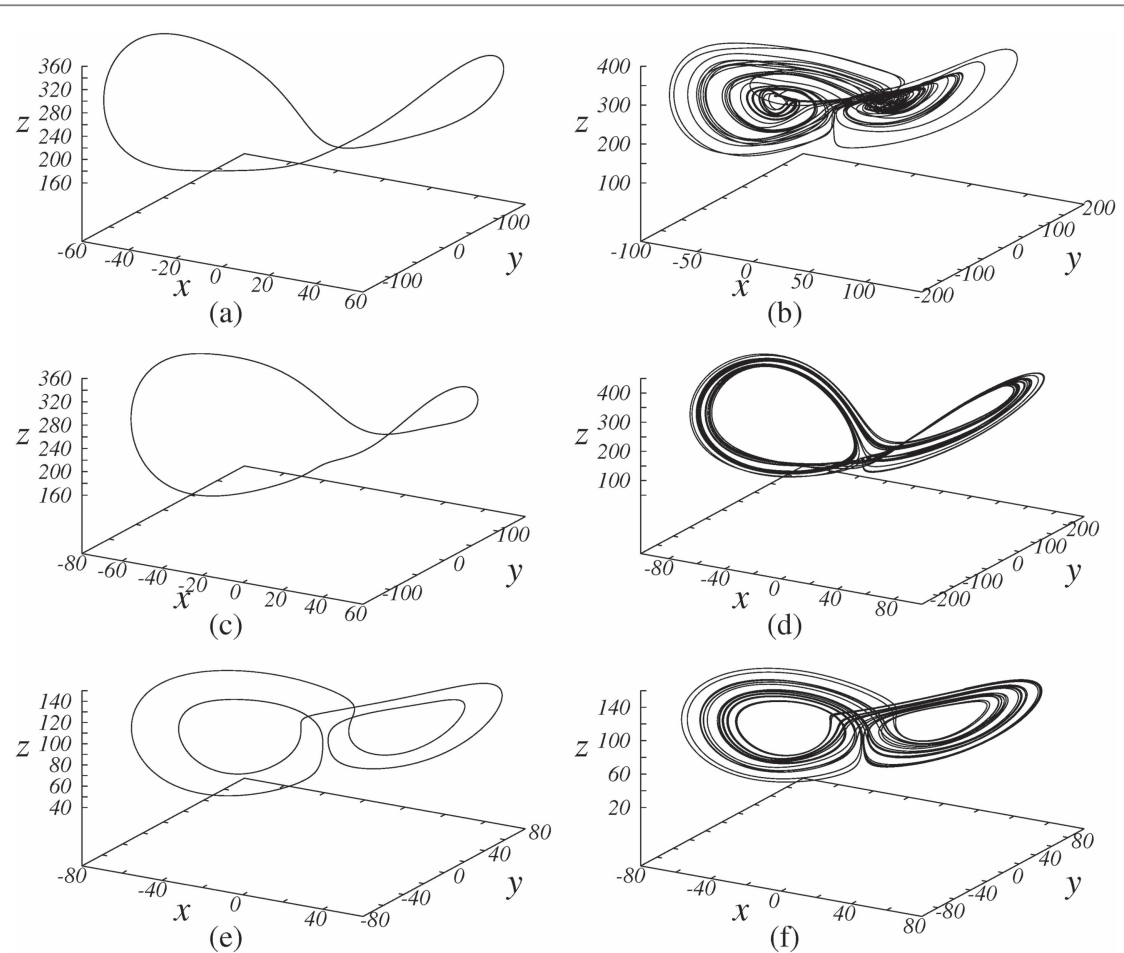


Figure 9. Six xyz projections of attractors related to the six-dimensional Lorenz system (3). (a), (c), and (e) Periodic trajectories, corresponding respectively to a point in the more prominent stripe in figures 7(a), (b), and (c) (see text). (b), (d), and (f) Chaotic trajectories, corresponding respectively to a point in the yellow to red region in figures 7(b), (d), and (f) (see text).

hyperchaotic regions with different number of positive Lyapunov exponents in parameter planes of the 6LM (5LM) here investigated, are taken into account four (three) complementary diagrams for each pair of parameters.

Figure 10 shows five (r, σ) parameter plane diagrams, displaying stability domains for the 5LM in (a), (b), and for the 6LM in (c), (d), (e). Diagrams in figure 10 were constructed by considering the second LLE in figures 10(a) and (c), the third LLE in figures 10(b) and (d), and the fourth LLE in figure 10(e). It is important to note that the LLE itself was considered in the construction of the diagrams in figures 4(a) and 7(a), respectively for the 5LM and the 6LM.

This work deals with five- and six-dimensional continuous-time dynamical systems, namely the 5LM and the 6LM. Therefore, when the LLE is greater than zero, there is still the possibility of having at most two (three) more positive Lyapunov exponents in the 5LM (6LM) case. As a consequence, can be investigated the occurrence of hyperchaos with two, and three positive Lyapunov exponents for the 5LM, and with two, three, and four positive Lyapunov exponents for the 6LM. For instance, a hyperchaotic region with four positive Lyapunov exponents in the (r, σ) parameter plane of the 6LM, would be associated with a common region colored in yellow to red in figures 7(a), 10(c), (d), and (e), while a hyperchaotic region with three positive Lyapunov exponents in the (r, σ) parameter plane of the 5LM, would be associated with a common region colored in yellow to red in figures 4(a), 10(a), and (b). According to what is said above, a closer look in figures 4(a) and 7(a) and in diagrams of figure 10, supports the conclusion that hyperchaotic behavior is not present in the (r, σ) parameter plane of the 5LM and the 6LM, at least in the investigated range of parameters. Regions painted in yellow to red are not observed in diagrams of figure 10.

On the other hand, a hyperchaotic region may be observed in both (r, b) and (σ, b) parameters planes of the 6LM. Figure 11 shows these parameter planes, constructed by considering the second LLE in (a) and (d), the third LLE in (b) and (e), and the fourth LLE in (c) and (f). The LLE itself was considered in the construction of the

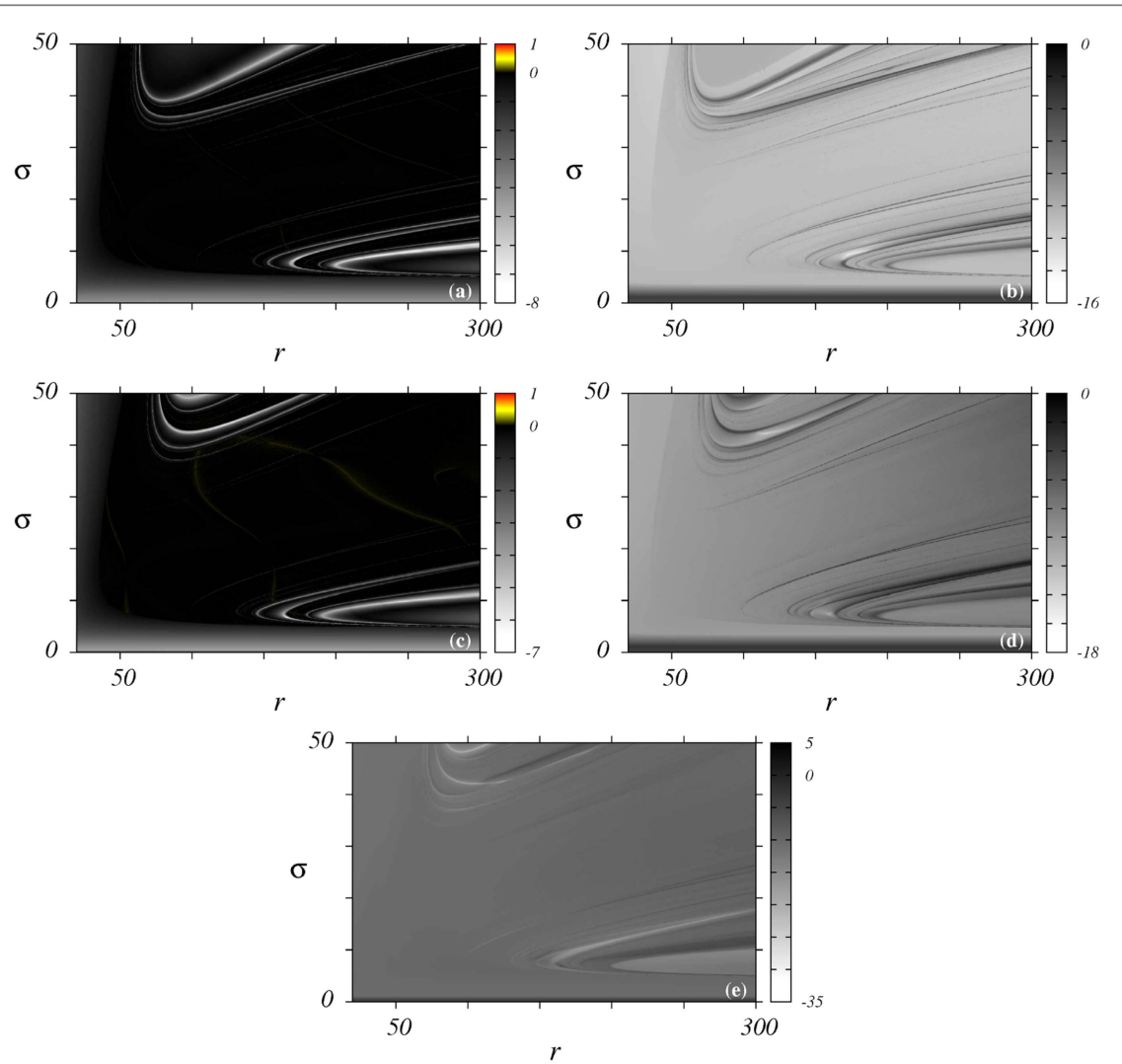


Figure 10. Regions of different dynamical behaviors in the (r, σ) parameter plane. (a), (b) The second and the third LLE for the 5LM. (c), (d), (e) The second, the third, and the fourth LLE for the 6LM.

diagrams in figures 7(b) and (c), respectively for (r, b) and (σ, b) parameter planes. By interpreting diagrams in figure 11, together the ones in figures 7(b) and (c), we conclude that the parameters associated with the yellow to red region in figures 11(a) and (d) characterize the dynamical behavior of the 6LM as hyperchaotic with two positive Lyapunov exponents. It is also possible to conclude that the 6LM does not display hyperchaos with three or four positive Lyapunov exponents. We point out that our investigation of hyperchaos in the 5LM took into account also the other two pairs of parameters not addressed in figure 10, namely (r, b) and (σ, b) . For both pairs of parameters were constructed diagrams similar to that appearing in figure 11 considering the second and the third LLE for the 5LM. Hyperchaotic regions were not observed. Therefore, as we have seen, hyperchaotic regions have not been verified in parameter planes of the 5LM, while have been observed in the (r, b) and (σ, b) parameter planes of the 6LM.

3. Conclusions and summary

Here we will summarize the conclusions already presented throughout the text, concerning the comparison of the cases involving the 5LM and the 6LM, with the 3LM case. With respect to the parameter planes regions, the area characterized by chaotic behavior is increased when we consider both the generalized Lorenz models. The range of the LLE is increased, as well as their upper limit, except for the case involving the parameters (r, b) for the 5LM, and (r, σ) for the 6LM. A larger r is necessary for the onset of chaos, when this parameter is thought of as the bifurcation parameter. This behavior is repeated when we consider any of the others parameters, namely b and σ , as the bifurcation parameter. The geometric shape of the attractors is preserved, regardless of whether they are

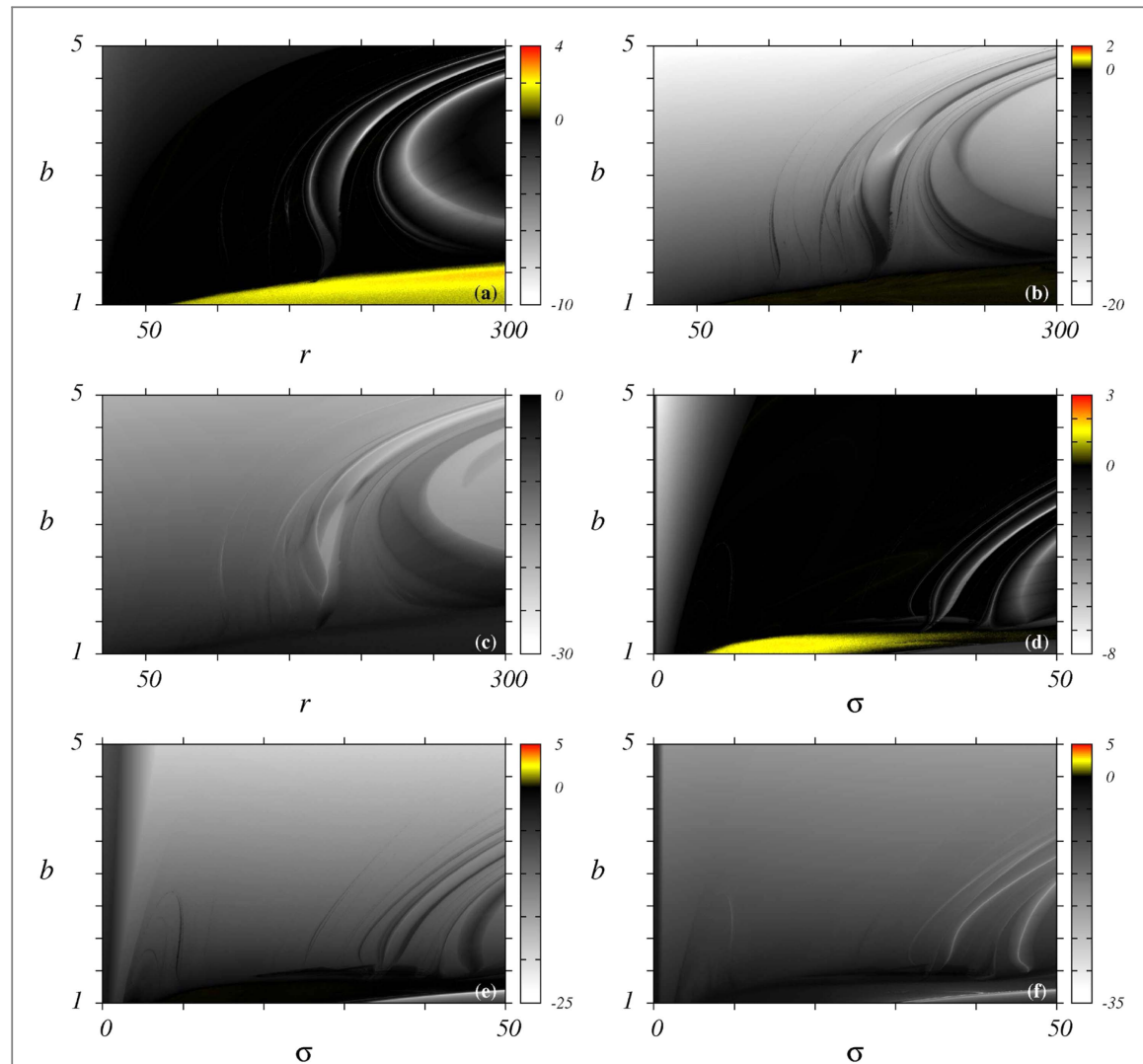


Figure 11. Regions of different dynamical behaviors in the (r, b) and (σ, b) parameter planes of the 6LM. (a), (d) The second LLE. (b), (e) The third LLE. (c), (f) The fourth LLE.

chaotic or periodic. Hyperchaotic regions have not been verified in parameter planes of the 5LM, while have been observed in the (r, b) and (σ, b) parameter planes of the 6LM.

In summary, we investigate numerically five- and six-dimensional Lorenz models. Numerical simulations were performed on two-dimensional parameter planes of both systems which are modeled, respectively, by a set of five and six autonomous, three-parameter, first-order nonlinear ordinary differential equations. By comparing with the classical three-dimensional Lorenz model, we show that for σ and b kept fixed a larger r results for the onset of chaos in five-and six-dimensional Lorenz models. The shape of bifurcation diagrams, periodic and chaotic attractors are preserved. We also show that hyperchaos is an observable dynamical behavior in the six-dimensional Lorenz model, and not in the five-dimensional Lorenz model.

Acknowledgments

The authors thank Conselho Nacional de Desenvolvimento Científico e Tecnológico-CNPq, and Fundação de Amparo à Pesquisa e Inovação do Estado de Santa Catarina-FAPESC, Brazilian Agencies, for financial support.

ORCID iDs

Paulo C Rech  <https://orcid.org/0000-0003-2235-0469>

References

- [1] Saltzman B 1962 *J. Atmos. Sci.* **19** 329
- [2] Lorenz E 1963 *J. Atmos. Sci.* **20** 130
- [3] Dullin H R, Schmidt S, Richter P H and Grossmann S K 2007 *Int. J. Bifurcation Chaos* **17** 3013
- [4] Barrio R, Blesa F and Serrano S 2009 *Physica D* **238** 1087
- [5] Gallas J A C 2010 *Int. J. Bifurcation and Chaos* **20** 197
- [6] Albuquerque H A, Rubinger R M and Rech P C 2008 *Phys. Lett. A* **372** 4793
- [7] Bonatto C and Gallas J A C 2008 *Phys. Rev. Lett.* **101** 054101
- [8] Albuquerque H A and Rech P C 2012 *Int. J. Circ. Theor. Appl.* **40** 189
- [9] Bonatto C and Gallas J A C 2007 *Phys. Rev. E* **75** 055204
- [10] Krüger T S and Rech P C 2012 *Eur. Phys. J. D* **66** 12
- [11] Li X F, Andrew Y T L and Chu Y D 2012 *Chin. Phys. Lett.* **29** 010201
- [12] Mathias A C and Rech P C 2012 *Neural Netw.* **34** 42
- [13] da Silva R A and Rech P C 2015 *Appl. Math. Comput.* **254** 9
- [14] Stegemann C and Rech P C 2014 *Int. J. Bifurcation and Chaos* **24** 1450023
- [15] Prants F G and Rech P C 2014 *Eur. Phys. J. B* **87** 196
- [16] Rech P C 2015 *Int. J. Bifurcation and Chaos* **25** 1530035
- [17] Rech P C 2016 *Phys. Scr.* **91** 075201
- [18] de Souza S L T, Batista A M, Baptista M S, Caldas I L and Balthazar J M 2017 *Physica A* **466** 224
- [19] Rech P C 2017 *Phys. Scr.* **92** 045201
- [20] Wiggers V and Rech P C 2017 *Int. J. Bifurcation and Chaos* **27** 1730023
- [21] Wiggers V and Rech P C 2017 *Chaos Solit. Fract.* **103** 632
- [22] Wolf A, Swift J B, Swinney H L and Vastano J A 1985 *Physica D* **16** 285
- [23] Leonov G A and Kuznetsov N V 2007 *Int. J. Bifurcation Chaos* **17** 1079
- [24] Butcher J C 2008 *Numerical Methods for Ordinary Differential equations* (New York: Wiley)
- [25] Barrio R and Serrano S 2007 *Physica D* **229** 43
- [26] Barrio R, Blesa F and Serrano S 2012 *Int. J. Bifurcation Chaos* **22** 1230019
- [27] Sparrow C 1982 *The Lorenz equations: Bifurcations, Chaos, and Strange Attractors* (Berlin: Springer)
- [28] Shen B W 2014 *J. Atmos. Sci.* **71** 1701
- [29] Shen B W 2015 *Nonlin. Processes Geophys.* **22** 749
- [30] Correia M J and Rech P C 2012 *Appl. Math. Comput.* **218** 6711
- [31] Rech P C 2014 *Appl. Math. Comput.* **247** 13